# Modeling of pancake frying with non-uniform heating source applied to domestic cookers

F. Sanz-Serrano[a],*, C. Sagues[a], A.H. Feyissa[b], J. Adler-Nissen[b], S. Llorente[c]

*[a]I3A Universidad de Zaragoza, Mariano Esquillor s/n, Zaragoza 50018, Spain*

*[b]Food Production Engineering, National Food Institute, Søltofts Plads, Building 227, 2800 Kgs. Lyngby, DTU, Denmark*

*[c]Research and Development Department, Induction Technology, Product Division Cookers,*
*BSH Home Appliances Group, Avenida de la Industria 49, Zaragoza 50016, Spain*

**Abstract**

The design of domestic cooking stoves is usually optimized by performing time-consuming cooking experiments, often using frying of pancakes as a standard. Simulation of cooking processes may reduce the number of experiments used in the development of the cooking stoves, saving time and resources. In this work we propose a model of contact frying of pancakes in domestic cookers, particularly in induction hobs and radiant cookers, in which the heating of the cooking vessels can be non-uniform. This non-uniformity is unavoidable in practice, but it can be reduced by optimizing the design of the cooker. The proposed model combines heat and mass transfer phenomena, and also includes the correlation between the browning development and the temperature distribution, the local water content and the cooking time. The model has been also validated through experiments using a commercial induction hob and a radiation stove. With this model the color of the cooked pancakes can be predicted, taking into account also uneven heating, and through simulations the design of the cooker can be improved.

*Keywords*: Modeling; pancake frying; non-uniform heating; browning development; domestic cooking.

## 1. Introduction

⁎ Corresponding author. Tel.:+34-669-917-886.

*E-mail addresses*: fer.sanz@unizar.es (F. Sanz-Serrano), csagues@unizar.es (C. Sagues), abhfe@food.dtu.dk (A.H. Feyissa), jadn@food.dtu.dk (J. Adler-Nissen), sergio.llorente@bshg.com (S. Llorente).

21    It is widely known that a non-uniform heating of the base of an even well-designed frying pan results in a non-

22    uniform cooking of the food, where overcooked zones as well as raw zones may appear. This undesirable effect is

23    critical and must be taken into account when designing cooking stoves, because the type and configuration of the

24    heating source determines the resultant temperature distribution in the pan.

25    In the case of induction cooktops, due to the geometry of the coil, a non-uniform current density distribution is

26    induced in the pan material (Carretero et al., 2015; Pham et al., 2012), which may cause significant temperature

27    gradients. This temperature unevenness is aggravated under certain common cooking conditions in the users'

28    kitchens. For example, when the cooking vessel is bigger than the coil, the outer area of the base remains colder than

29    the center.

30    As a part of the quality control of the induction hobs, manufacturers perform different tests with each hob variant

31    under real cooking conditions, such as contact frying of pancakes or steaks, deep frying of chips or croquettes and

32    water boiling (AEN/CT N 213 Electrodomesticos, 2014). These standardized tests are developed to evaluate

33    different features of the cooker performance, such as efficiency, energy consumption, durability or cooking

34    uniformity. The most common test used for the evaluation of the heating uniformity is pancake frying, in which the

35    temperature distribution is indirectly analyzed by studying the differences in the browning of the pancake face in

36    contact with the pan during the frying process. Such tests imply spending high amounts of time and resources, which

37    could be in fact reduced by using other direct methods for measuring the temperature distribution, such as an

38    infrared (IR) camera and heating an empty pan. However, the evaluation considering the food is necessary for

39    controlling the quality of the stoves, since the normal functioning in the final user's home is reproduced, and the

40    suitability of the cooker performance can easily be confirmed. For this reason the development of theoretical models

41    of different cooking situations is of great interest, since the result of the cooking experiments can be predicted in an

42    earlier stage of the design process, saving costs of prototypes and experiments. Since one of the most critical tests

43    for evaluating the cooking uniformity is the contact frying of thin pancakes, this type of food will be studied in the

44    present work.

45    Some contact frying models have been presented in previous works, where focus has been to study the food

46    properties such as heat conductivity, or to estimate the effects of the cooking process such as mass loss, local

47    temperature evolution or shrinkage effects. For example Zorrilla and Singh (2003) proposed a two-dimensional

48    model of contact frying of meat patties, Gupta (2001) studied the contact baking of flat Indian bread in a continuous

49    oven with a simplified model, Feyissa et al. (2011) proposed a theoretical model of contact frying of thick pancakes,

50    considering coupled heat and mass transfer phenomena. In all these works, the temperature distribution of the hot

51    surface (double grill, steel slats, baking plate) was uniform, which is the best-case situation in a contact cooking

52    process. However when considering a domestic cooker, the heat source typically provides a non-uniform heat

53    distribution, which may lead to an uneven temperature distribution in the cooking vessel. Hence, it becomes

54    necessary to include a non-uniform heat source in the new model.

55    As mentioned before, the evaluation of the heating uniformity of domestic cookers is carried out through the

56    experimental measurement of browning differences in cooked pancakes, which is not only a way of taking into

57    account the user's perception of quality, but also an indirect way of analyzing the temperature distribution in the

58    cooker, since browning is the consequence of the temperature evolution, time and product composition. The

59    browning of bakery products is the result of a combination of Maillard reactions and caramelization (Martins et al.,

60    2000; Purlis, 2010). The color formation in different types of food products using different cooking techniques

61    (meat, bread or biscuit) has been modeled with a basis in chemical kinetics theory and empirical correlations, giving

62    a good agreement between the measured color and the predicted color after a determined cooking process (Broyart

63    et al., 1998; Purlis and Salvadori, 2009). A similar approach can be used for modeling the color formation in a

64    contact frying process using a domestic stove, taking into account a non-uniform temperature distribution. Knowing

65    the evolution of the temperature and water content, the resulting color distribution at a given time may then be

66    predicted and used for the evaluation of the heating performance of the cooker.

67    The objective of the present work is to establish a pancake frying model which includes a non-uniform power

68    distribution transferred by a domestic cooker to the base of the cooking vessel. It allows the calculation of the

69    temperature and water content in the food as well as the resulting color distribution. This non-uniform heating

70    condition has barely been considered in previous works related to industrial applications of food engineering, where

71    the heating source and/or the cooking surface are usually designed in order to minimize the temperature gradients.

72    However in domestic cookers, due to the wide variability of types of pans existing in the market, a perfectly uniform

73    temperature distribution is often impossible to obtain. Therefore, the contributions of this work are the proposed

74    transport model with a non-uniform heat source and an experimentally determined color correlation between the

75 browning of the pancake surface and the frying process (temperature, water content and time). The proposed model

76 makes possible to simulate the frying process and obtain the color distribution, helping to predict if the configuration

77 of a certain cooker is optimal. This would improve the design process of cooktops and save development costs. In

78 order to adjust the proposed model, experiments of controlled cooking using a uniform-heating rig (Ashokkumar

79 and Adler-Nissen, 2011) have been carried out, and the obtained results have been extrapolated to the real case of

80 domestic cookers. The model has been also validated through experiments using a commercial induction hob and a

81 radiation stove.

82 **2. Theory**

83 The contact frying of pancakes can be modeled as a coupled heat and mass transfer problem (Feyissa et al.,

84 2011). The heat transferred from the base of the frying-pan to the pancake dough increases its temperature, and the

85 water present in the dough starts to evaporate, absorbing a high amount of energy during the phase change. The

86 gradient of the concentration of liquid water and vapor produces a mass transfer effect due to diffusion inside the

87 product, which also affects the thermal properties and, therefore, the temperature evolution.

88 *2.1. Two-dimensional model of pancake cooking*

89 The proposed model is based on the previous work from Feyissa et al. (2011), in which a one-dimensional model

90 of the heat and mass transfer problem for a thick pancake (8 mm) was presented. In the present work a two-

91 dimensional axisymmetric model is used, in order to include the non-uniform heating of the cooking vessel.

92 Moreover, the pancake thickness is closer to the traditional French pancake (3 mm thick) used in the standardized

93 tests. Like in Feyissa et al. (2011) it is assumed that the temperature-induced chemical reactions of the solid

94 components, such as the egg protein coagulation or the color formation, have no influence on the bulk material

95 properties. The model is implemented in COMSOL Multiphysics® 5.0, which is based on the Finite Element

96 Method (FEM) for the numerical simulations. This implementation allows the selection of the input conditions such

97 as the power source, and the material properties. Therefore similar models can be used to simulate the frying process

98 using different heating technologies. In this work an induction hob which directly heats the cooking vessel placed on

99 a ceramic glass plate has been considered (Fig. 1 (a)), but also a heating rig with a hot surface at uniform

100 temperature, used in the previous works by Ashokkumar and Adler-Nissen (2011) and by Feyissa et al. (2011), Fig.

101  1 (b). The uniform-heating rig model will be used to identify the model parameters and develop the color formation

102  correlations, and the results obtained can then be used in a more complex model with a non-uniform heating.

103  *2.1.1. Heat transfer model*

104  The thermal system which has been considered consists of a pancake product inside a frying disk with an outer

105  rim. The disk is placed on a ceramic glass plate in the case of the induction hob and on an aluminum slab in the case

106  of the uniform-heating rig (cf. also section 3.1.). The temperature evolution of the frying disk heated by induction is

107  given by the governing equation:

$$P + \lambda \, \nabla^2 T = \rho \, C \, \frac{\partial T}{\partial t} \tag{1}$$

108  where $P$ is the volumetric power density generated by the inductor in W/m$^3$. The second term is the effect of heat

109  conduction, where $\nabla^2 T$ is the Laplacian of the temperature $T$ in K and $\lambda$ is the heat conductivity of the material with

110  units W/(m $\cdot$ K). The term on the right side is the variation of the energy stored in the system with time, where the

111  material has density $\rho$ with units kg/m$^3$ and specific heat capacity $C$ with units J/(kg $\cdot$ K). The power term $P$

112  disappears in the case of the uniform-heating rig, since the heat is transferred to the disk through the contact with the

113  aluminum block, obtaining the governing equation:

$$\lambda \, \nabla^2 T = \rho \, C \, \frac{\partial T}{\partial t} \; . \tag{2}$$

114  The heat transfer within the pancake domain is given by equation (3):

$$\lambda_p \, \nabla^2 T = \rho_p \, C_p \, \frac{\partial T}{\partial t} + Q_{evp} \tag{3}$$

115  where $Q_{evp}$ in W/m$^3$ is the heat sink corresponding to the water evaporation, $\lambda_p$, $\rho_p$ and $C_p$ are the product

116  properties – the thermal conductivity, the density and the effective specific heat capacity, respectively.
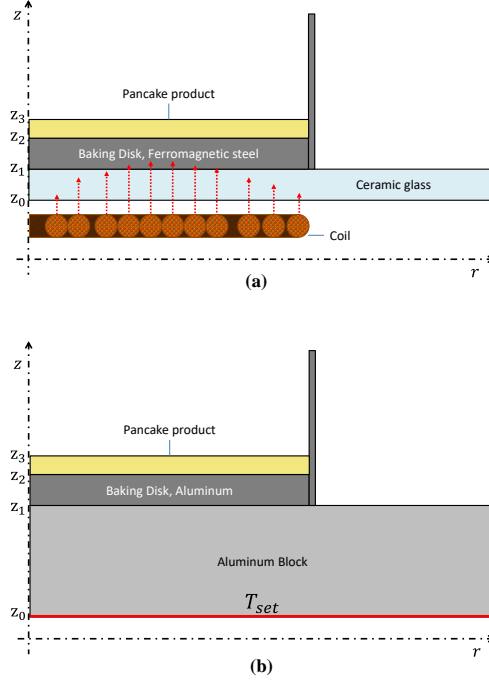
Fig. 1. Axisymmetric schemes of the pancake cooking model using different heating technologies: (a) induction heating with a non-uniform power distribution generated in the frying disk – symbolized with red arrows, (b) uniform-heating rig with aluminum block at controlled temperature $T_{set}$ on the highlighted surface.

The energy absorbed by the water during the evaporation process is calculated as:

$$Q_{evp} = R_{evp} \cdot L_{evp} \tag{4}$$

where $R_{evp}$ in kg/(m$^3$ · s) is the mass evaporation rate, which is a function of temperature and water content, and $L_{evp} = 2.26 \cdot 10^6$ J/kg is the water evaporation enthalpy at 100ºC and 1 atm. The evaporation rate $R_{evp}$ is described by:

$$R_{evp} = \sigma_{evp} \cdot \rho_p \cdot \theta(T) \cdot \eta(x_l) \tag{5}$$

where $\sigma_{evp}$ is the rate constant with units 1/s and $\theta(T), \eta(x_l)$ are functions used to model the complex phenomena which occur during the evaporation of the water in the pancake product. A similar expression to calculate $R_{evp}$ , based on the Arrhenius equation, was presented by Feyissa et al. (2011). However, two slight modifications have been carried out in the present work. Firstly, the phase change coefficient introduced by Feyissa et al. (2011) has been reformulated for convenience, obtaining the equivalent exponential function $\theta(\mathrm{T})$, parameterized by the

6

130  evaporation temperature $T_{ev} = 373.15$ K and the dimensionless constant $k_\theta$, as given by (6)

$$\theta(T) = \begin{cases} exp\left(k_\theta\left(1 - \dfrac{T_{ev}}{T}\right)\right) & 0 < T \leq T_{ev} \\ 1 & T_{ev} < T \end{cases}.$$  (6)

131  Secondly, instead of considering that the mass evaporation rate is proportional to the water content $x_l$, as stated in

132  the work of Feyissa et al. (2011), the piecewise function $\eta(x_l)$ is defined as:

$$\eta(x_l) = \begin{cases} 0 & 0 \leq x_l \leq x_{l_{bnd}} \\ 1 & x_{l_{bnd}} < x_l \leq 1 \end{cases}.$$  (7)

133  The threshold water content, $x_{l_{bnd}} = 0.4$, takes into account the effect of the bound water present in the dough

134  (Bushuk and Mehrotra, 1977; Ulbrich and Flöter, 2014) which cannot be evaporated during the cooking process.

135  Thus, the evaporation rate remains constant with the water content provided that free water is present, and the

136  evaporation stops when the threshold $x_{l_{bnd}}$ is reached, which is a more realistic approximation. In order to reduce

137  computational problems associated with sharp changes of the values of $\theta(T)$ and $\eta(x_l)$, smoothed piecewise

138  functions are used in the implementation in the FEM software.

139      In the case of the induction hob, the bottom surface of the glass ($z = z_0$) is considered adiabatic, because the

140  temperature of the coil and the air beneath the glass is close to the temperature of the glass, and the heat losses are

141  therefore negligible. In the case of the uniform-heating rig, the surface is documented to have a constant temperature

142  $T_{set}$ (Ashokkumar and Adler-Nissen, 2011).

143      The heat flux established through the bottom surface of the baking disk due to the contact with the ceramic glass

144  in the induction hob is defined with a contact conductance $h_c$ (Sanz-Serrano et al., 2016)

$$-\lambda_d \left.\frac{\partial T}{\partial z}\right|_{z=z_1} = -\lambda_g \left.\frac{\partial T}{\partial z}\right|_{z=z_1} = h_c \left.(T_g - T_d)\right|_{z=z_1}$$  (8)

145  where $T_d$, $T_g$ and $\lambda_d$, $\lambda_g$ are the temperatures and heat conductivities of disk and glass, respectively. Equivalently,

146  the contact conduction between the frying disk and the hot aluminum slab of the rig is

$$-\lambda_d \left.\frac{\partial T}{\partial z}\right|_{z=z_1} = -\lambda_s \left.\frac{\partial T}{\partial z}\right|_{z=z_1} = h_c \left.(T_s - T_d)\right|_{z=z_1}$$  (9)

147  where $T_s$ and $\lambda_s$ are the temperature and heat conductivity of the hot slab.

148 On the disk top surface ($z = z_2$), in contact with the pancake, the heat flux continuity is considered, which is given

149 by equation (10)

$$-\lambda_d \frac{\partial T}{\partial z}\bigg|_{z=z_2} = -\lambda_p \frac{\partial T}{\partial z}\bigg|_{z=z_2} \quad . \tag{10}$$

150 On the top surface of the pancake and the glass (or the aluminum slab), and on the wall of the frying disk, heat

151 losses due to natural convection and radiation are considered. The corresponding heat transfer coefficients are

152 calculated from conventional empirical correlations by the FEM software, considering the geometry and ambient

153 temperature (Bergman et al., 2011). For the pancake surface the convection coefficient is 8 W/m²K, on the walls of

154 the frying disk and on the glass (or the aluminum slab) the convection coefficient is 10 W/m²K. The emissivity of

155 the different materials is: 0.96 for the pancake (similar to water), 0.1 on the steel walls, 1 on the glass and 0.3 on the

156 aluminum slab.

157 *2.1.2. Mass transfer model*

158 The mass transfer phenomenon only takes place inside the pancake domain and through the top surface of the

159 pancake, in which the liquid water and vapor move mainly due to diffusion. The governing equations are similar to

160 those appearing in Feyissa et al. (2011)

$$\rho_p \frac{\partial x_l}{\partial t} = \nabla \cdot \left( \rho_p \, D_l \nabla x_l \right) - R_{evp} \tag{11a}$$

$$\rho_p \frac{\partial x_v}{\partial t} = \nabla \cdot \left( \rho_p \, D_v \nabla x_v \right) + R_{evp} \tag{11b}$$

161 where $x_l + x_v + x_s = 1$ is a constraint. The mass fractions of the solid, liquid and vapor are $x_s$, $x_l$, $x_v$, expressed in

162 kg of water/kg of sample, respectively. The diffusion coefficients are $D_l$, $D_v$ with units m² s$^{-1}$, $R_{evp}$ is the rate of

163 water evaporation (which is water disappearance or the vapor generation rate), as defined in (5).

164 A null mass flux is considered through the boundaries in contact with the frying disk, and through the top surface

165 of the pancake a mass flow of vapor is stated as the boundary condition

$$-D_v \frac{\partial x_v}{\partial z}\bigg|_{z=z_3} = k_v \cdot \rho_p \cdot \left( x_v - x_{v_a} \right)\bigg|_{z=z_3} \tag{12}$$

166 where $k_v$ is a mass flux constant with units m/s and $x_{v_a}$ is the humidity of the surrounding air, expressed in basis of

167    product mass, being $x'_{v_a}$ the measured humidity in kg of vapor per kg of air and $\rho_a$ the air density at ambient

168    temperature

$$x_{v_a} = x'_{v_a} \frac{\rho_a}{\rho_p}. \tag{13}$$

169    *2.1.3. Calculation of thermal properties*

170        The thermal properties of the metal and the glass do not change significantly during the frying process. However,

171    there is a strong dependence of the product properties with the water and vapor content, which change continuously

172    due to the evaporation and mass transport phenomena. Thus, the local values of the pancake properties are

173    calculated as a function of temperature and composition, which is stated by the mass fractions of the solid, liquid

174    and vapor: $x_s$, $x_l$, $x_v$, solution of the mass transfer problem. The solid fraction is the aggregate of solid components

175    in the dough (protein, fat, carbohydrate), obtained from the pancake recipe and from the food database of Saxholt et

176    al. (2008).

177        To calculate the product density $\rho_p$, additive volumes are considered in the following expression extracted from

178    (Nesvadba, 2014)

$$\rho_p = \left( \frac{x_l}{\rho_l} + \frac{x_s}{\rho_s} + \frac{x_v}{\rho_v} \right)^{-1} \tag{14}$$

179    $\rho_l$ and $\rho_s$ are the densities of the liquid water and the solid. The porosity (volume fraction of vapor) $\varepsilon_v$ is obtained

180    with

$$\varepsilon_v = \frac{x_v}{\rho_v} \rho_p = x_v \frac{R_g \cdot T}{pA \cdot M_w} \rho_p \tag{15}$$

181    where the ideal gas law is used in the calculation of the vapor density $\rho_v$, considering atmospheric pressure $pA =$

182    1atm (Datta, 2007a), the gas constant $R_g = 8.2 \cdot 10^{-2}$ atm L mol$^{-1}$ K$^{-1}$ and the molecular weight of vapor $M_w =$

183    18 g mol$^{-1}$. The local expansion of the pancake due to the additional volume filled with vapor can be calculated

184    with

$$\alpha = \frac{x_{s_0} \cdot \rho_{p_0}}{x_s \cdot \rho_p} \tag{16}$$

185    where $x_{s_0}$, $\rho_{p_0}$ are the initial solid mass fraction and the initial density.

186    The heat capacity $C_p$ and the heat conductivity $\lambda_p$ of the pancake are calculated with well-known expressions

187    according to Nesvadba (2014)

$$C_p = \sum_i x_i \, C_i$$

$$\frac{1}{\lambda_{p_\perp}} = \sum_i \frac{\varepsilon_i}{\lambda_i}$$

$$\lambda_{p_\parallel} = \sum_i \varepsilon_i \cdot \lambda_i \tag{17}$$

$$\lambda_p = g_\lambda \cdot \lambda_{p_\perp} + (1 - g_\lambda) \cdot \lambda_{p_\parallel}$$

188    where $\varepsilon_i$ is the volume fraction and $\lambda_i$ is the heat conductivity of each component. The value of the factor $g_\lambda$

189    depends on the porosity with the expression

$$g_\lambda = 0.04 + g_\varepsilon \cdot \varepsilon_v \tag{18}$$

190    which is similar to the one appearing in Nesvadba (2014) for porous food products. The sensitivity of the results is

191    significant with respect to the coefficient $g_\varepsilon$ and its value must be determined experimentally.

192    *2.2. Browning development model*

193    The browning is the result of a combination of Maillard reactions and caramelization (Martins et al., 2000; Purlis,

194    2010). The evaluation of the progress of the browning process can be conveniently carried out with computer vision

195    systems, in which the variation of the color of the product surface is obtained from image processing tools. This

196    technique has recently become more common due to the advantages which offers with respect to other chemical

197    methods (Zheng et al., 2006). In particular, the lightness parameter L\* of the standard color space CIE L\*a\* b\* is

198    normally used (Gökmen et al., 2008; León et al., 2006; Zheng et al., 2006).

199    The Maillard reactions and the caramelization occur simultaneously and they can be integrated in a combined

200    model, which relates the color with the time, temperature and water content of the product (Purlis, 2010). In this

201    work, the browning model is based on first-order kinetics with the browning rate constant depending on temperature

202    and water content. The variation of the color component L\* with time, as presented by Purlis (2010), is given by

$$\frac{dL^*}{dt} = -k \, L^* \tag{19}$$

203    where $k$ is the browning rate constant, which depends on the temperature as stated in the Arrhenius' law

$$k = k_0 \, exp\left(-\frac{A}{T}\right) \tag{20}$$

204    being $k_o$ and $A$ variables dependent on the water content in kg of water / kg of sample

$$k_0 = k_1 + \frac{k_2}{x_l}$$
$$A = A_1 + \frac{A_2}{x_l} \tag{21}$$

205      As it is known, the temperature and the water content also vary with time during the cooking process. However

206    they can be calculated by means of the aforementioned numerical method based in FEM. For this reason, the

207    solution of (19) can be obtained with the expression

$$L^* = L_o \, exp\left(\int_{t_0}^{t} -k_0 \, exp\left(-\frac{A}{T}\right) dt\right) \tag{22}$$

208    which can be numerically obtained knowing the evolution of $T$ and $x_l$ with the time. The parameters, $L_0$, $k_1$, $k_2$,

209    $A_1$, $A_2$ will be identified using experimental measurements of the color of pancakes cooked with the uniform-

210    heating rig, using different cooking times and temperatures. For the remaining color components in the L*a*b*

211    space, the suitability of similar equations with different parameter values will be discussed in section 3.3.

212    **3. Experiments**

213      The values of the parameters $\sigma_{ev}, k_\theta, g_\varepsilon, k_v, h_c, D_l, D_v$ which appear in the previously presented model of heat

214    and mass transfer and the aforementioned parameters of the browning development model are unknown and

215    therefore must be determined experimentally. In order to simplify the problem and increase the accuracy of the

216    identification process, the experiments are performed using the aforementioned uniform-heating rig which provides

217    a surface at a controlled, uniform temperature (Ashokkumar and Adler-Nissen, 2011). Under this condition the

218    problem is simpler, as the effect of the uneven temperature distribution in the pan is avoided, and the color

219    formation in the bottom surface of the pancake can be related to the controlled temperature.

220    *3.1. Experimental set-up*

221      The uniform-heating rig (Fig. 2) consists of a slab of aluminum of 30x30x2.5 cm$^3$ with isolated side faces and

222    heated from beneath by contact with an electric hotplate. Inside the slab there is a temperature probe, which feeds

223    back data to a controller which allows the setting of the desired temperature (Ashokkumar and Adler-Nissen, 2011).

224    The equipment rests on an electronic balance, with a precision of 0.1 g, and this allows the continuous recording of

225    the mass loss. The frying disk employed in these experiments is an aluminum disk of 9 cm of diameter and 0.5 cm

226    of thickness, with a non-stick PTFE coating, and the wall is a ring of stainless steel of the same internal diameter,

227    2.5 cm of height and 0.15 cm of thickness (Feyissa et al., 2015, 2011).

228
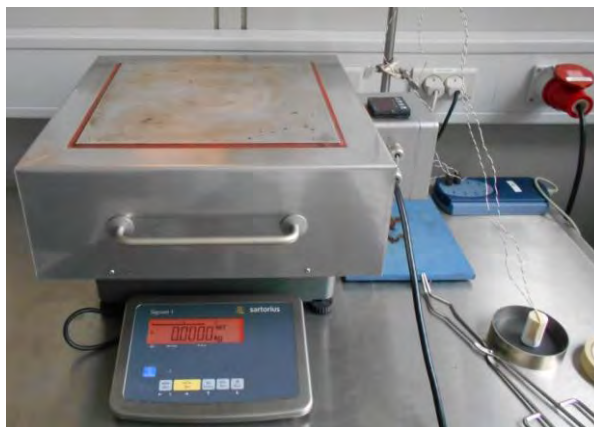


229    Fig. 2. Uniform-heating rig and balance.

230    In order to measure the pancake temperature, type T thermocouples of 0.75 mm of diameter are used with a PICO

231    TC08 register. Two thermocouples are fixed through a cylindrical piece of PTFE with drills at the bottom and at 3.5

232    mm from the bottom. With this disposition the evolution of the temperature of the disk and of the top surface of the

233    pancake can be measured. The bottom thermocouple is fixed to the disk surface 12 mm from the center, using

234    thermo-resistant tape (KAPTON) and thermal conductive silicone, in order to improve the thermal contact between

235    the sensor and the surface, Fig. 3. The PTFE piece fixates the thermocouples in the desired position. Due to its low

236    conductivity ($0.25\ \mathrm{W/(m \cdot K)}$), similar to the pancake dough, it has little disturbing effect on the cooking process.

237    The pancake dough is prepared with the ingredients which appear in the standard (AEN/CT N 213

238    Electrodomesticos, 2014), which includes milk (53.3%), chicken egg (20.7%), wheat flour (25.8%) and salt (0.2%).

239    The initial density is measured by weighing a known volume of dough, obtaining $\rho_{p_0} = 1110\ \mathrm{kg/m^3}$ . The initial

240    water content, estimated from the product composition and the water content of the constituents, appearing in

241    Saxholt    et    al.,    (2008)    is    $x_{l_0} = 0.65\ \mathrm{kg\,water/kg\,sample}$,    and    the    solid    mass    fraction    is    $x_{s_0} =$

242  0.35 kg solid/kg sample.

243  The desired temperature is set in the control unit of the uniform-heating rig and it is allowed to equilibrate for 20

244  minutes. The standard states that the temperature of the frying disk should be 235ºC±5ºC for a right cooking result.

245  However in order to obtain a wider range of data different temperatures are tested, between 180ºC and 260ºC. This

246  range is defined considering the temperature differences which can appear when heating a frying pan with an

247  induction hob in a normal cooking process. The higher limit is stated due to the maximum temperature which the

248  PTFE coating resists without starting to degrade (Fluoroproducts, 1996).



249
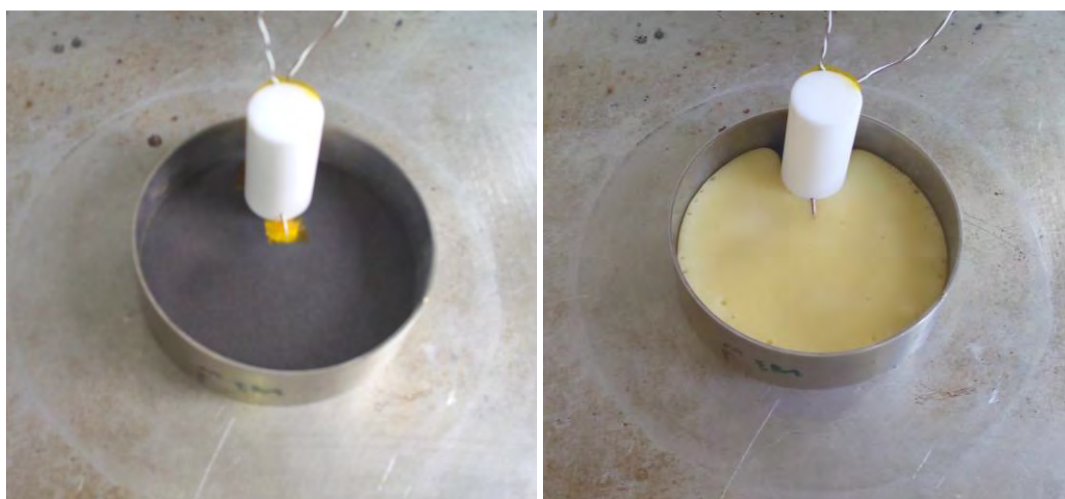
250  Fig. 3. Frying disk with type-K thermocouples and PTFE piece. The left picture shows the position of the bottom sensor fixed to the disk surface.
251  The right picture shows the other sensor measuring the temperature on the top surface of the pancake during the cooking process.

252  The frying disk with the cylindrical PTFE piece with the thermocouples inside (Fig. 3) is placed on the hot

253  surface. When the disk temperature is steady, the scales is set to zero and the dough is poured as fast as possible

254  using a syringe, trying to spread it uniformly. After a given time the pancake is removed from the disk and it is

255  placed inside a dark chamber, where a picture of the bottom face is taken with a conventional digital camera (no

256  flash, velocity ISO-80, focal 3.2mm, exposure time 1/640s). Different cooking times are tested, from 60 s to 240 s,

257  in order to measure the influence of the time in the browning development. The expansion of the pancakes cannot be

258  measured with enough accuracy, as from the same instant in which they are taken out from the frying pan they start

259  to shrink due to cooling and loss of stored vapor. Moreover the expansion is not completely uniform and different

260  thicknesses were observed. Therefore, the expansion is calculated theoretically; cf. eq. (16) in section 2.1.

261 *3.2. Measurement of temperature, mass and water content*

262     The measured temperatures inside the pancakes prepared on the uniform-heating rig at different surface

263 temperatures from 180ºC to 260ºC, are shown in Fig. 4. The temperatures measured with the bottom thermocouple

264 (solid lines) and the thermocouple at the top surface of the pancake at a height of 3.5 mm (dashed lines), are

265 presented. The total cooking time in this case is 240 seconds. The bottom temperature curves exhibit an initial drop

266 when the cold pancake dough is poured on the frying disk, where after they slowly rise towards the rig temperature,

267 as expected. The temperature measured by the top thermocouple before pouring the dough presents a higher value

268 with respect to the real ambient temperature, 25ºC, due to the heating of the PTFE piece which holds it. The pancake

269 top surface approaches the water evaporation temperature, because this phase change consumes a high amount of

270 energy and produces a cooling effect. As the pancake dries out, the evaporation effect is lower, and the temperature

271 may exceed the evaporation temperature, as it is the case of a set temperature of 260ºC. No appreciable separation of

272 the sensor from the top surface due to dough expansion was noticed during any experiment, and the repeatability of

273 the measurements was also confirmed by comparison of the results obtained in different pancakes, cooked with

274 same set temperatures of the uniform-heating rig, at different instants. This confirms that if there is some

275 displacement, it has low influence, or it is the same in all experiments.
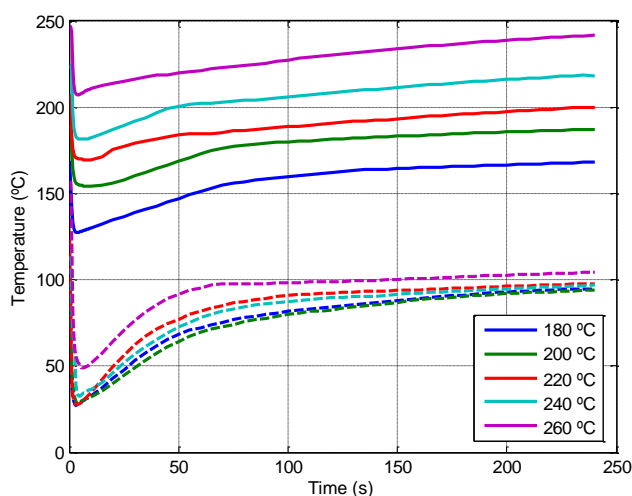


276

277 Fig. 4. Temperature evolution measured on the bottom surface of the pancake (continuous lines) and on the top surface of the pancake (dashed
278 lines) using different temperatures of the uniform-heating rig.

279     As an example of the mass measurement, Fig. 5 shows the evolution of the normalized pancake mass during a

14

280    cooking process with different set temperatures from 180ºC to 260ºC, during 240s. The initial mass used for the

281    normalization was measured with a conventional analytical balance as the difference between the mass of the

282    syringe before and after pouring the dough. The jagged behavior of the presented lines is a consequence of

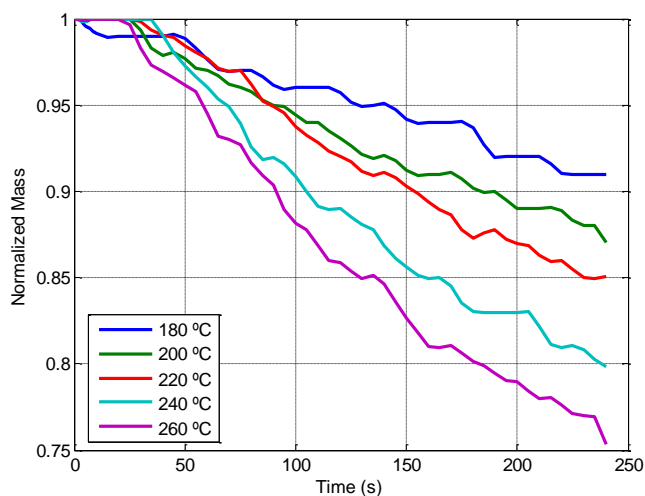283    oscillations of the weight measurement and the posterior median filter employed to eliminate spurious data.



284

285    Fig. 5. Pancake total mass measured during the cooking process, using different temperatures of the uniform-heating rig.

286    *3.3. Color extraction from computer vision system*

287    The pictures of the pancakes are processed using Matlab in order to extract the browning information. A blue-

288    colored background was employed in order to help the segmentation of the picture and obtain the colors of the

289    pixels corresponding to the pancake. As it can be seen in Fig. 6, which corresponds to a pancake cooked using a set

290    temperature of 240ºC during 180s, there is a wide variation of colors on the pancake surface, which is the result of

291    the production of bubbles of water vapor in the interphase of the pancake product and the plate. These bubbles with

292    different sizes generate insulation layers which slow down the increment of temperature in some zones of the

293    product, producing a lower browning with respect to other zones which remained in contact with the plate. The

294    regions of interest are the zones constantly in contact with the frying plate, and this must be taken into account in the

295    color extraction process, since the color correlation is modeled from the evolution of the temperature measured on

296    the disk surface.

15

297

Fig. 6. Picture of a pancake cooked using a set temperature of 240ºC during 180s in the uniform-heating rig. Images scale is 380 pixels per inch, the color space is sRGB.

Each picture is processed using the same algorithm in Matlab R2013a. First, a color space conversion from the original sRGB to the standard CIE L*a*b* is carried out. Then with the b* component a mask is obtained, which is used to suppress the image background. In order to extract the color which truly corresponds to the measured temperature, a region of interest is defined by segmentation, suppressing the lighter areas. The normalized histograms of the color components in the region of interest are shown in Fig. 7. The Gaussian curve which best fits each distribution is also plotted, as well as the mean value calculated with the distribution data (red vertical line). It can be seen that the mean of the Gaussian and the calculated mean are almost coincident, which confirms the good approximation of the normal distribution.

The mean values obtained for each color component L*, a* and b*, depending on the plate temperature and the time are shown in Fig. 8. The values have been converted to the commonly used range for the CIE L*a*b* color space, in which L* ranges from 0 to 100, and a*, b* range from -128 to 127. The blue lines correspond to experiments at the same cooking time in the temperature graphs (left-hand), and at the same temperature in the time graphs (right-hand). A different behavior of each component can be noticed. The only component which is strictly decreasing with time and temperature, according to the proposed model, is the component L*. In the case of a* and b* the tendency differs, and expression (22) is not adequate to explain the behavior of these color components. Thus, for simplification the values of a* and b* are calculated as the mean value of the experimental data.
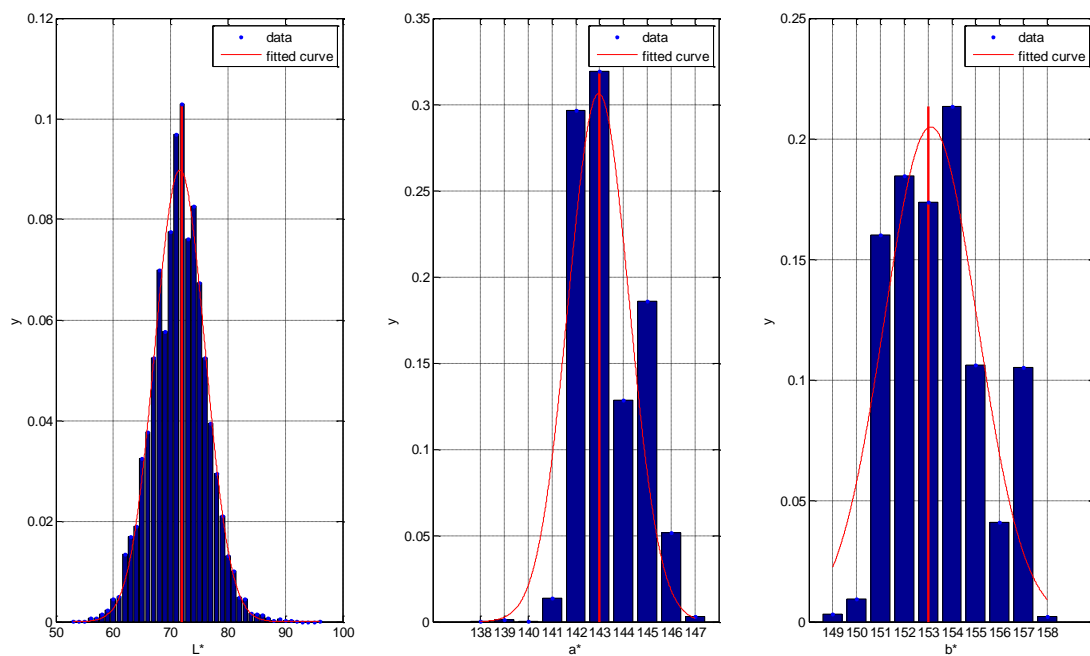
316

Fig. 7. Histograms of each color component obtained from the regions of interest. The Gaussian distribution which best fits each histogram is shown.
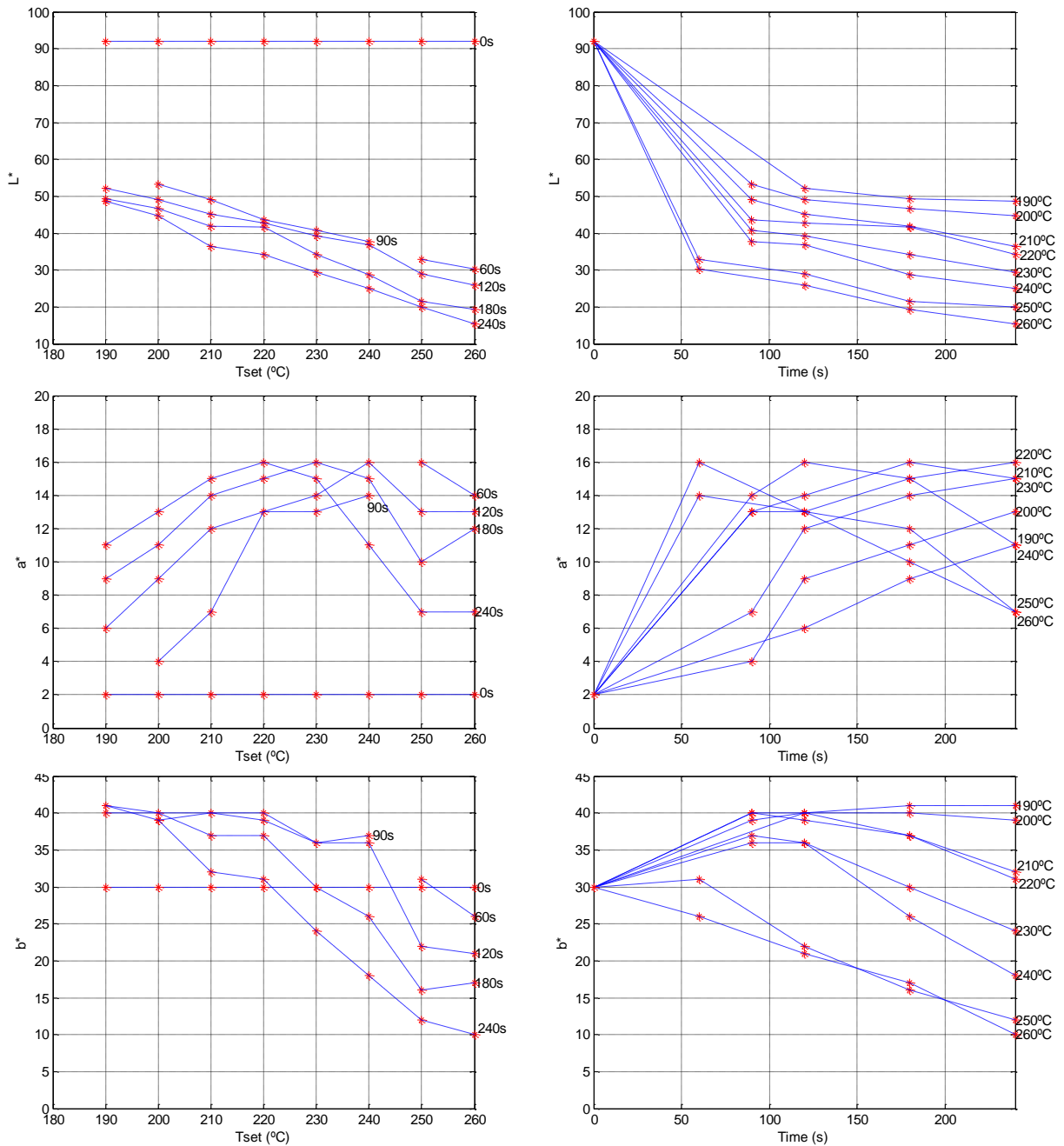
317
318

319

320

Fig. 8. Mean value of each measured color component L\*a\*b\* depending on the set temperature and the cooking time. Blue lines represent data obtained from experiments with the same time on the left-hand plots, and with the same set temperature on the right-hand plots.

### 3.4. Parameter identification

The experimental data collection is used in the identification process of the heat and mass transfer model parameters and of the color correlation parameters. Because each model can be simulated independently, the

18

326      identification of each set of parameters is carried out separately.

327      *3.4.1. Optimization for the finite element model COMSOL-Matlab*

328      An optimization algorithm is implemented in Matlab in order to calculate the values of the model parameters

329      which best fit the experimental measurements of temperature and mass loss. The algorithm uses the COMSOL-

330      Matlab interface, and the optimization method used is the non-linear least squares method, using a trust-region-

331      reflective algorithm. The objective function to minimize is the sum of the squared errors between the measured and

332      calculated evolution of the temperature on top and bottom of the pancakes and of the normalized mass, taking into

333      account different experiments with set temperature from 180 ºC to 260 ºC.

334      The built-in COMSOL modules "Heat transfer in solids" and "Transport of concentrated species" are used for

335      modeling the cooking process. A time-dependent study solves the transient problem for the desired time. The model

336      geometry is relatively simple, therefore a mapped mesh has been used in the whole model. A finer mesh is

337      employed in the domain corresponding to the pancake, where the coupled thermal and mass transfer problem is

338      solved, with elements of 1 mm in radial direction and 0.23 mm in axial direction. In the disk domain the elements

339      are bigger in axial direction (1.25 mm), since heat conduction is higher and low temperature differences are

340      expected. The total number of elements is 2207 domain elements plus 512 boundary elements. The time step is set

341      to 1s, though for the first steps the software takes a lower time step of 1e-3s, which is increased as convergence is

342      achieved. The selected solver is direct, fully coupled, with the default configuration given by the software.

343      The optimization variables and the obtained values are presented in Table 1. Examples of the fitting are shown in

344      Fig. 9, in which the temperature evolution in the top and bottom surface of the pancake and the normalized mass are

345      plotted for two set temperatures: 180ºC and 260ºC. The simulated curves are plotted as continuous lines, and the

346      experimental data with asterisks. The good fitting of calculated and measured data demonstrates the accuracy of the

347      results. The small differences in the normalized mass may be a consequence of having considered constant values of

348      the diffusion coefficients for the vapor and liquid water, instead of including the effects of pressure or temperature,

349      as presented by Datta (2007b). These coefficients determine the mass fraction of vapor which is contained inside the

350      pancake (and the porosity), which affects the heat conductivity and the rate of water evaporation.

351      *3.4.2. Optimization of color model L\*a\*b\**

352      For the calculation of the parameters of the browning development model, the measured temperature evolution

353 and the water content in the bottom surface of the pancake are employed. The water content is calculated using the

354 finite element model for different set temperatures. The optimization algorithm uses equations (21) and (22) to

355 minimize the error between the calculated and the measured color component L* for each cooking time and set
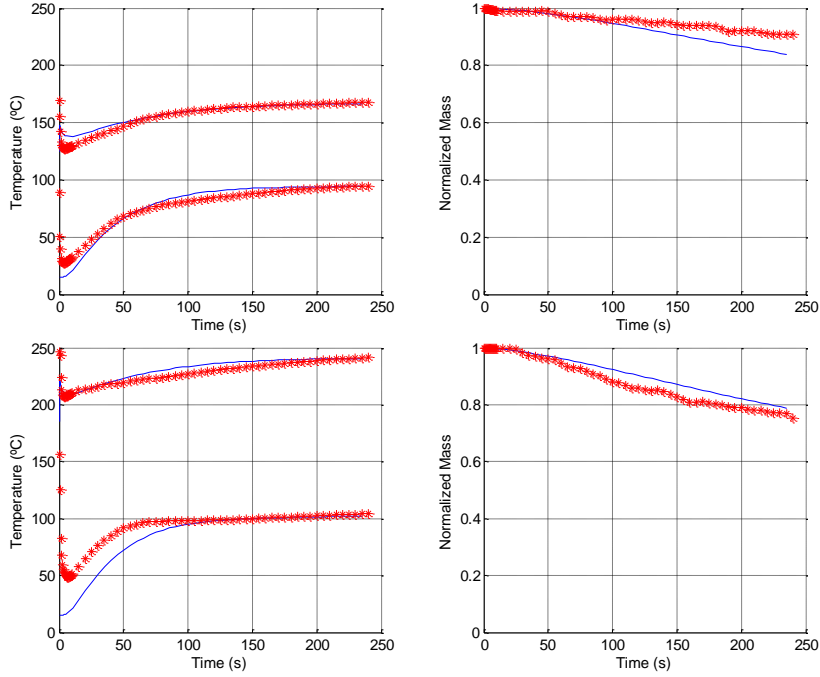
356 temperature.

357



358 Fig. 9. Comparison of measured and calculated temperature and mass evolution using the parameter values from the identification algorithm, for
359 different set temperatures: 180ºC and 260ºC.

360 Table 1. Parameter values obtained from the optimization algorithm.

| Parameter | Value | Units |
|---|---|---|
| $\sigma_{ev}$ | 5.44e-4 | $s^{-1}$ |
| $k_\theta$ | 1.61e3 | - |
| $g_\varepsilon$ | 1.2 | - |
| $k_v$ | 3.8e-3 | $m \cdot s^{-1}$ |
| $h_c$ | 460 | $W \cdot m^{-2} \cdot K^{-1}$ |
| $D_l$ | 1e-9 | $m^2 \cdot s^{-1}$ |
| $D_v$ | 1.05e-5 | $m^2 \cdot s^{-1}$ |

361

362 The fitted curves can be seen in Fig. 10, which shows the dependence of the color value with the cooking time

363    and the set temperature as a parameter. The error between the fitted curves and the measured values is a result of the

364    high dispersion of the measured data and the approximation of the proposed model based on reaction kinetics. The

365    parameter values for the fitting of the L* component, and the mean values of a* and b* are shown in Table 2. With

366    these values, the correlations can be used to simulate the color distribution when cooking the pancake in an

367    induction hob with known power distribution.



368
369
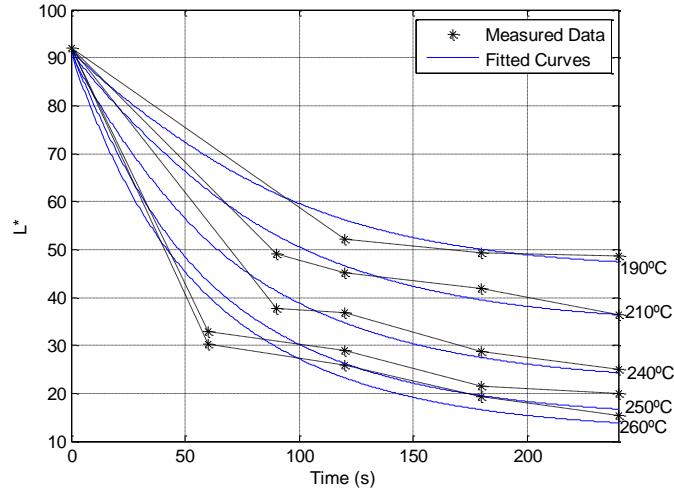
370    Fig. 10. Fitting of the color component L* obtained using the parameters obtained from the identification.

371

372    Table 2. Parameter values for the correlations of color component L* and mean values of color components a* and b*.

| Parameter | Value | Units |
|-----------|-------|-------|
| $L_0$ | 92 | - |
| $k_1$ | 15.4 | $s^{-1}$ |
| $k_2$ | 2.22e-14 | $s^{-1}$ |
| $A_1$ | 2.22e-14 | K |
| $A_2$ | 2.16e3 | K |
| $a^*$ | 12.6 | - |
| $b^*$ | 32.7 | - |

373

21

374 **4. Application of the model to pancake cooking in non-uniform heating domestic cookers**

375     Considering that the pancake behavior is independent of the source which heats the cooking vessel, the proposed

376 two-dimensional model of pancake cooking can be used for different types of heating technologies in domestic

377 stoves. To achieve this, the heat source needs to be well characterized, so that it can be used as an input in the

378 model.

379     As an example, two different commercial stoves are considered: an induction hob (BOSCH PIE645B18E) and a

380 radiant stove (Balay 3EE721LS). The induction hob consists of a coil of diameter 18 cm, heating a conventional

381 frying pan of 19 cm, made of ferromagnetic steel with known thermal and electromagnetic properties. The power

382 distribution generated in the pan can be calculated (Carretero et al., 2015; Sanz-Serrano et al., 2016) and used

383 directly in the finite element model proposed in this work. As it can be seen in Fig. 11 (left), the power distribution

384 is not completely uniform: the heat generation is null in the center and outside the coil, which may cause unevenness

385 in the temperature distribution. The radiant stove has a cooker composed of two independent resistors in concentric

386 configuration. The internal has a diameter of 12 cm and the external a maximum diameter of 21 cm. The power

387 distribution, transferred by conduction from the ceramic glass to the frying pan, is shown in Fig. 11 (right) (Sanz-

388 Serrano et al., 2016). In this case the frying pan has a diameter of 21 cm, the same as the external resistor in the
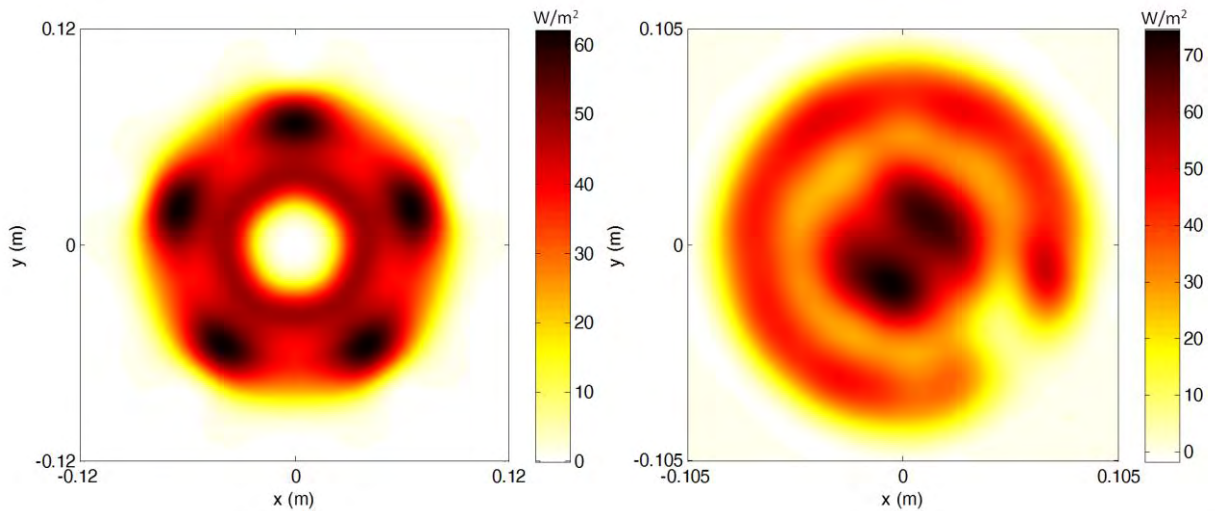
389 cooking zone.

390



391 Fig. 11. Power distribution generated in a C-45 ferromagnetic steel disk of diameter 24 cm with a conventional induction cooker with a coil of 18
392 cm of diameter (left); power distribution transferred from the ceramic glass to a frying pan in a double cooker of 12/21 cm of an electric stove
393 (right).

394  A cooking situation supplying a total power of 1000 W to a pan of 19 cm of diameter with the mentioned

395  inductor is simulated, and the pancake color is predicted. Since the power distribution is not completely

396  axisymmetric and slightly fluctuates in the angular direction, the average power distribution in this direction is

397  computed and the radial profile is used in the model. The radial profiles of normalized power distribution,

398  temperature of the bottom of the frying pan, and L* component of the color distribution obtained from the

399  simulation after 60s are shown in Fig. 12 (left). Since the pan diameter is bigger than the coil diameter, the heating

400  of the outer area is insufficient, obtaining high temperature gradients in the base of the pan and an inadequate

401  cooking result, shown by the differences in the predicted color of the pancake. It can also be noticed that despite the

402  center of the pan is not directly heated by the coil, the heat conduction from the hotter area towards the center helps

403  to make uniform in the temperature.

404  A cooking process with a frying pan of 21 cm of the same material used for the induction hob is simulated with

405  the radiant stove as the heating element. The average in angular direction of the power distribution shown in Fig. 11

406  (right) is also computed and used as input in the model. The power needed for cooking is lower than in the case of

407  the induction cooker, provided that the ceramic glass has been previously heated up to the normal operation

408  temperature (around 450ºC); therefore the power considered is 600 W, supplied continuously during time. The radial

409  profiles of power distribution and temperature in the bottom of the frying pan, and the L* color component obtained

410  are shown in Fig. 12 (right). In this case, the power distribution is higher in the central part of the cooker, due to the

411  unequal power transferred by each one of the resistances. This generates a higher temperature difference in the

412  center of the pan with respect to the border, compared with the induction cooker. The resulting color distribution

413  follows the same behavior as the temperature. The maximum difference obtained in the L* value is 43, which is

414  similar to the maximum difference obtained for the induction hob, 37. However, the deviation for the electric stove

415  is higher, which makes the color distribution less uniform, producing a perception of lower quality in the cooking

416  result, as can be seen in Fig. 13.

417  In order to assess these simulation results obtained with the proposed model, a set of 16 pancakes are cooked

418  using each one of the aforementioned stoves. For the induction hob, the power supplied by the inductor is 1000 W

419  and the cooking time for the first face of the pancake is 60 s (afterwards the pancakes are flipped and further cooked

420  during 15 s). For the radiant cooker, the average power supplied by the resistors is 600 W and the cooking time for

the first face of the pancake is 70 s (as the pan is slightly bigger in this case). It can be considered that the color distribution on the first face remains constant after cooking the second face. A picture of one of the pancakes, and the values of the different color components L*a*b* along four radii taken every 90º are shown in Fig. 14 for the induction hob, and in Fig. 15 for the radiant cooker. The simulated color components have been also plotted in black continuous line for comparison, showing good agreement in the L* component.

The measured colors present a noisy behavior due to the irregular surface of the pancakes and the small vapor bubbles which alter the contact between the product and the frying pan during the cooking process. A lighter color area near the center of the pancake, effect of a bigger vapor bubble, can also be seen in the case of the induction hob, which is similar to the effects observed in the experiments with the uniform-heating rig, shown in Fig. 6. The appearance of these bubbles seems to have a random occurrence, therefore their location cannot be predicted with the proposed model. However, since they provide no information about the uniformity of the temperature distribution, they should be disregarded for the evaluation of the cookers. Using the model for the calculation of the color distribution in different situations, the color differences are computed instead of measured, avoiding also the effect of differences in the evaluator's perception.

It is evident from the simulation that the color distribution is closely related to the temperature distribution in the pan during the cooking process. Therefore, it might be possible to test the heaters' design by measuring the temperature of the surface of an empty pan for example using an IR camera. However in order to correctly evaluate the heating uniformity it is necessary to account for the effect of the food on the pan temperature and, despite the robustness of the camera measurement, it is impossible to measure the temperature distribution in the pan while the food is being prepared. Moreover, the temperature distribution measured at a given time is not as representative as the measurement or calculation of the final color distribution, which depends on the whole temperature history during the cooking process.
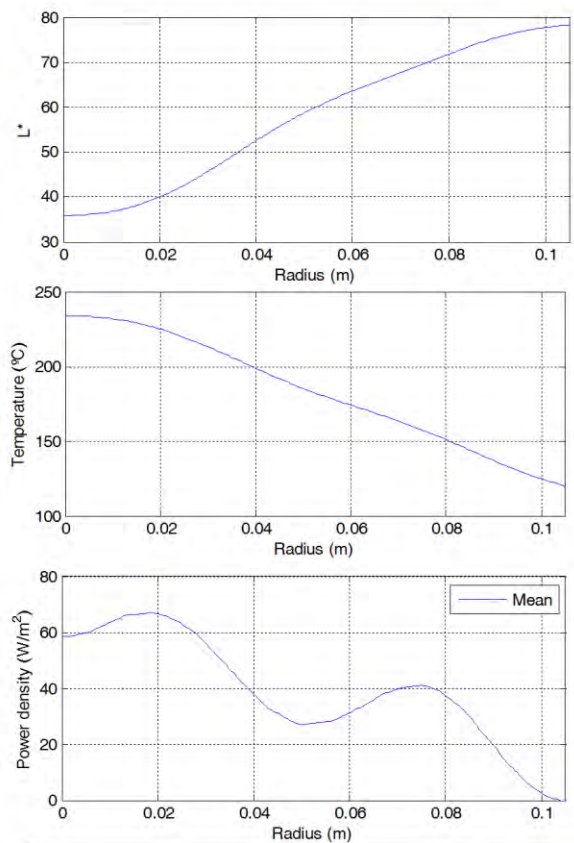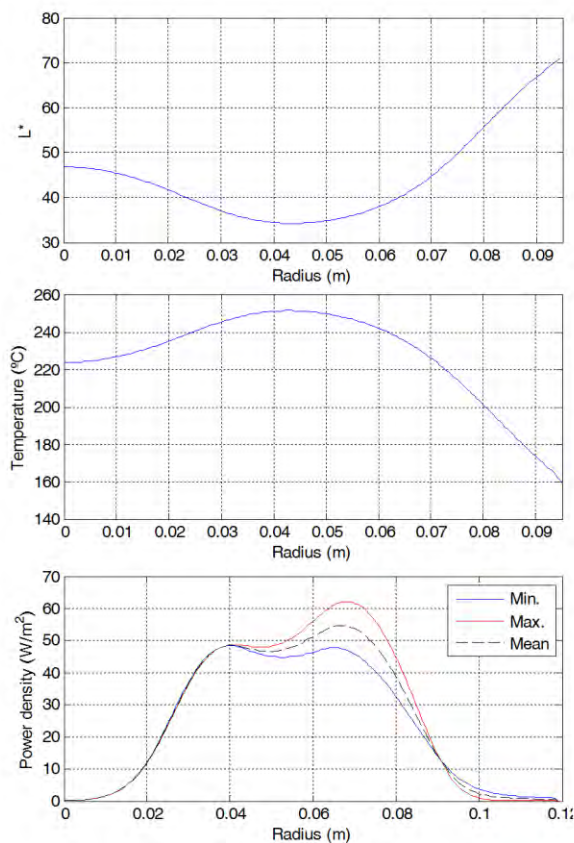
443

Fig. 12. Radial profiles of power density distribution, temperature in the bottom of the frying pan and L* component obtained from simulation of a cooking process with: an inductor of 18 cm heating a 19 cm pan during 60s supplying 1000 W (left); a double radiant cooker of 12/21 cm heating a 21 cm pan (right) during 70s supplying 600W.
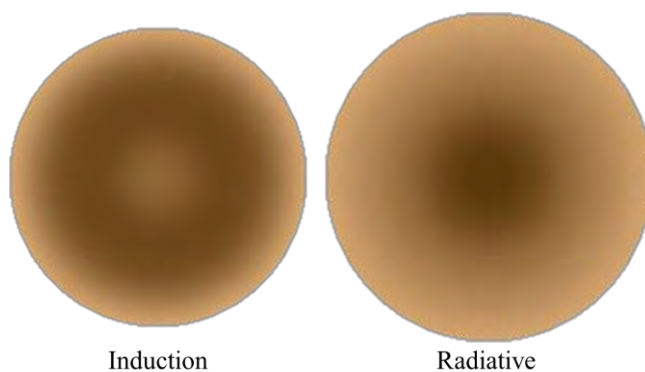


447

Fig. 13. Simulated pancakes for an induction cooker and an electric stove, using the same type of frying pan and cooking time. The color is obtained from the conversion of calculated L*a*b* to RGB for visualization.

25

450
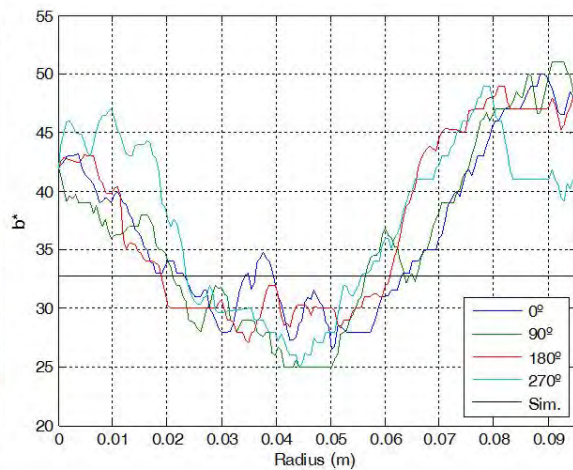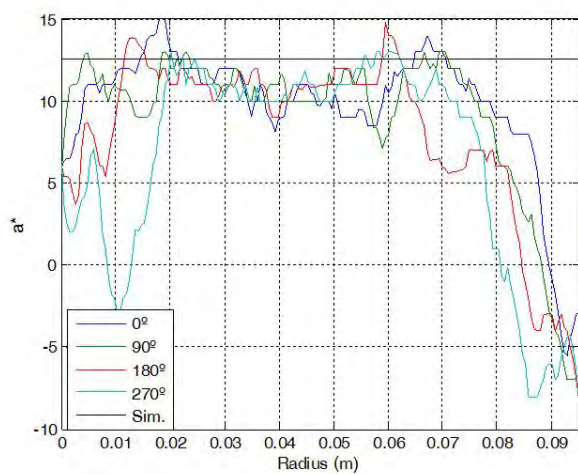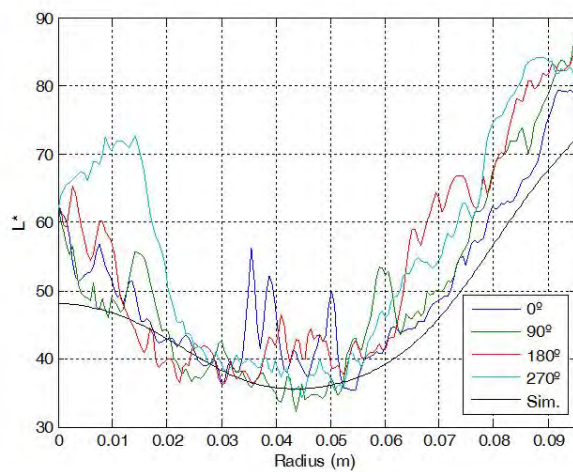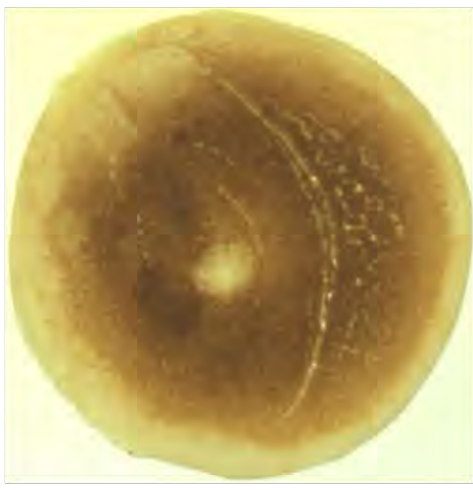
Fig. 14. Pancake cooked in a pan of 19 cm of diameter made of ferromagnetic steel heated with an inductor cooker of 18 cm. Radial profiles of color components L*a*b* measured and simulated.
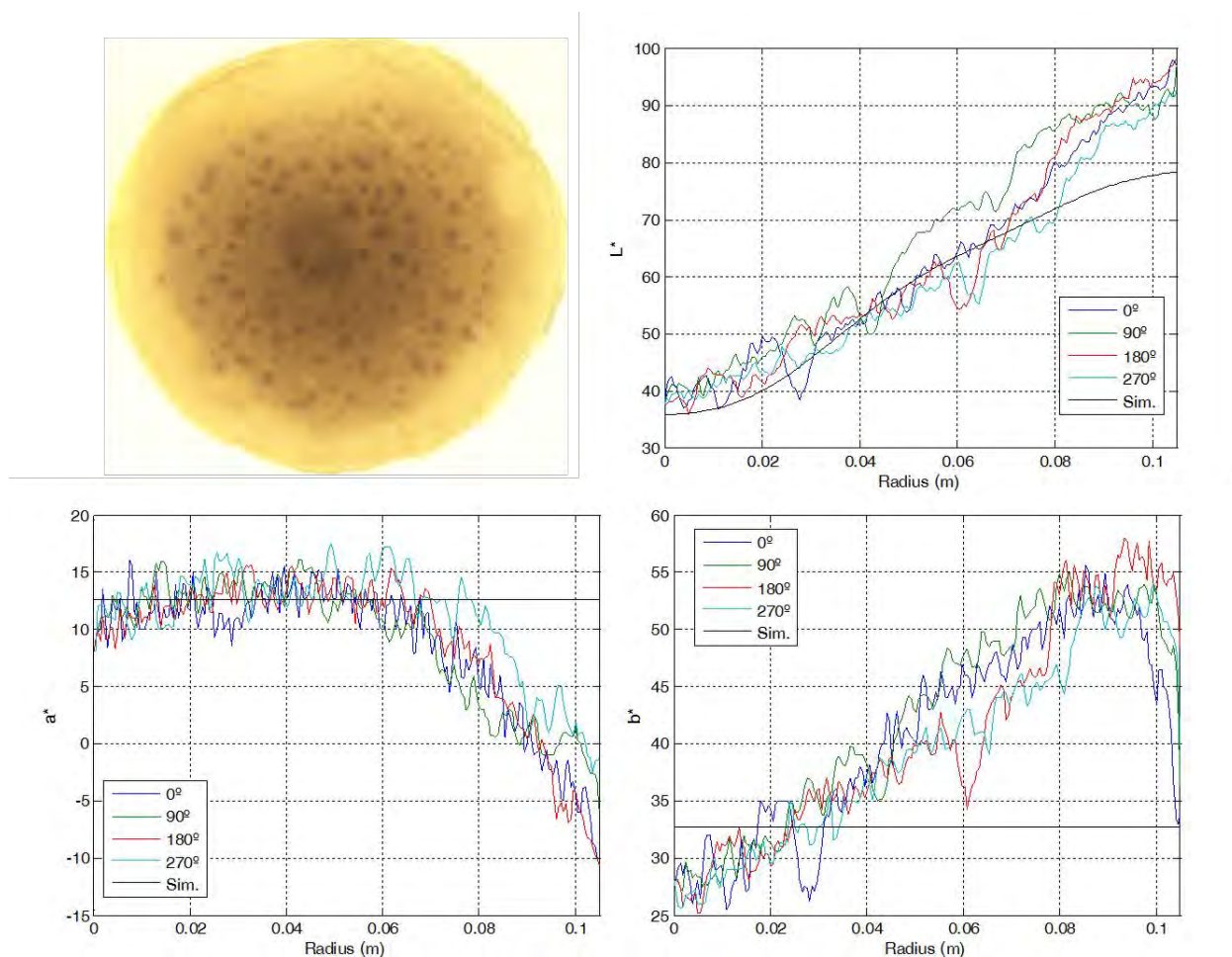
451
452

453

454

Fig. 15. Pancake cooked in a pan of 21 cm of diameter made of ferromagnetic steel heated with a double radiant cooker of 12/21 cm. Radial profiles of color components L*a*b* measured and simulated.

## 5. Conclusions

A two-dimensional model of heat and mass transfer and browning development in pancake cooking has been proposed. The main contribution of this work is the consideration of a non-uniform heating in the modeling, inspired by the real situation existing in current domestic cookers. Thus, the influence of the type of heating source and the frying pan are also included in the model. Moreover combining a transport model and a browning development model gives a more complete tool for the study of the contact pan-frying process.

The proposed model can be used for predicting the cooking result when using a given domestic cooker with a non-uniform heating in the food. Thus, the performance of such a stove can be evaluated without developing a real prototype and testing it experimentally, saving costs and accelerating the design process. In this work a particular

induction cooker and a radiant cooker of an electric stove have been considered, however alternative configurations and technologies could be further studied.

The color correlations of the browning development show a good agreement in the L* component. The evolution of the a* and b* components with the cooking process is relatively small but also non-linear, and its behavior cannot be represented by the selected model based on first order kinetics. However the average value calculated from the experimental data can be used to reproduce the changes in the browning when predicting the pancake color. The insulating effect of vapor bubbles in the interphase between the frying pan and the dough on the color was observed in the experiments. The light-color zones produced by these bubbles cannot be predicted with the proposed model, however since their appearance seem to be independent of the heating uniformity of the cooker, it is reasonable to ignore them for the evaluation of the cooker performance. The maximum color difference obtained for the induction cooker and the radiant cooker is similar, despite the color distribution with the first one is more uniform. In general, if the power is distributed towards the outer area of the pan, the cooking result is better than if it is concentrated in the center.

As future work, the model could be also used to evaluate different features of interest of the cooking process which are difficult to measure, such as the local temperature evolution and water content distribution, the energy employed in the water evaporation, the influence of the materials employed in the cooking vessel over the cooking efficiency or the effect of modifying the dough recipe.

**Acknowledgements**

**References**

490 AEN/CT N 213 Electrodomesticos, 2014. Household electric cooking appliances - Part 2: Hobs - Methods for measuring performance.
491    http://www.aenor.es/aenor/normas/normas/fichanorma.asp?tipo=N&codigo=N0054329

492 Ashokkumar, S., Adler-Nissen, J., 2011. Evaluating non-stick properties of different surface materials for contact frying. J. Food Eng. 105, 537–
493    544. doi:10.1016/j.jfoodeng.2011.03.018

494 Bergman, T.L., Lavine, A.S., Incropera, F.P., Dewitt, D.P., 2011. Fundamentals of heat and mass transfer, seventh ed. ed, Dekker Mechanical
495    Engineering. John Wiley & Sons.

496 Broyart, B., Trystram, G., Duquenoy, A., 1998. Predicting colour kinetics during cracker baking. J. Food Eng. 35, 351–368. doi:10.1016/S0260-
497    8774(98)00021-1

498 Bushuk, W., Mehrotra, V.K., 1977. Studies of Water Binding by Differential Thermal Analysis. II. Dough Studies using the Melting Mode.
499    Cereal Chem. 54, 320–325.

500 Carretero, C., Acero, J., Alonso, R., Burdio, J., 2015. Normal Mode Decomposition of Surface Power Distribution in Multiple Coil Induction
501    Heating Systems. IEEE Trans. Magn. 52, 1–1. doi:10.1109/TMAG.2015.2487883

502 Datta, A.K., 2007a. Porous media approaches to studying simultaneous heat and mass transfer in food processes. II: Property data and
503    representative results. J. Food Eng. 80, 96–110. doi:10.1016/j.jfoodeng.2006.05.012

504 Datta, A.K., 2007b. Porous media approaches to studying simultaneous heat and mass transfer in food processes. I: Problem formulations. J.
505    Food Eng. 80, 80–95. doi:10.1016/j.jfoodeng.2006.05.013

506 Feyissa, A.H., Christensen, M.G., Pedersen, S.J., Hickman, M., Adler-Nissen, J., 2015. Studying fluid-to-particle heat transfer coefficients in
507    vessel cooking processes using potatoes as measuring devices. J. Food Eng. 163, 71–78. doi:10.1016/j.jfoodeng.2015.04.022

508 Feyissa, A.H., Gernaey, K. V., Ashokkumar, S., Adler-Nissen, J., 2011. Modelling of coupled heat and mass transfer during a contact baking
509    process. J. Food Eng. 106, 228–235. doi:10.1016/j.jfoodeng.2011.05.014

510 Fluoroproducts, D., 1996. Teflon PTFE Fluoropolymer Resin: Properties Handbook. DuPont Fluoroproducts.

511 Gökmen, V., Açar, Ö.Ç., Arribas-Lorenzo, G., Morales, F.J., 2008. Investigating the correlation between acrylamide content and browning ratio
512    of model cookies. J. Food Eng. 87, 380–385. doi:10.1016/j.jfoodeng.2007.12.029

513 Gupta, T.R., 2001. Individual heat transfer modes during contact baking of Indian unleavened flat bread (chapati) in a continuous oven. J. Food
514    Eng. 47, 313–319. doi:10.1016/S0260-8774(00)00135-7

515 León, K., Mery, D., Pedreschi, F., León, J., 2006. Color measurement in L*a*b* units from RGB digital images. Food Res. Int. 39, 1084–1091.
516    doi:10.1016/j.foodres.2006.03.006

517 Martins, S.I.F.S., Jongen, W.M.F., Van Boekel, M. a J.S., 2000. A review of Maillard reaction in food and implications to kinetic modelling.
518    Trends Food Sci. Technol. 11, 364–373. doi:10.1016/S0924-2244(01)00022-X

519 Nesvadba, P., 2014. Thermal properties of unfrozen foods, in: Engineering Properties of Foods. Taylor & Francis Group, pp. 223–245.

520 Pham, H.N., Fujita, H., Ozaki, K., Uchida, N., 2012. Estimating Method of Heat Distribution Using 3-D Resistance Matrix for Zone-Control
521    Induction Heating Systems. IEEE Trans. Power Electron. 27, 3374–3382. doi:10.1109/TPEL.2011.2179984

522 Purlis, E., 2010. Browning development in bakery products - A review. J. Food Eng. 99, 239–249. doi:10.1016/j.jfoodeng.2010.03.008

523 Purlis, E., Salvadori, V.O., 2009. Modelling the browning of bread during baking. Food Res. Int. 42, 865–870. doi:10.1016/j.foodres.2009.03.007

524 Sanz-Serrano, F., Sagues, C., Llorente, S., 2016. Inverse modeling of pan heating in domestic cookers. Appl. Therm. Eng. 92, 137–148.
525    doi:10.1016/j.applthermaleng.2015.09.084

526 Saxholt, E., Christensen, A.T., Møller, A., Hartkopp, H.B., Hess Ygil, K., Hels, O.H., 2008. Danish Food Composition Databank, revision 7
527    [WWW Document]. Dep. Nutr. Natl. Food Institute, Tech. Univ. Denmark. URL http://www.foodcomp.dk/

528 Ulbrich, M., Flöter, E., 2014. Impact of high pressure homogenization modification of a cellulose based fiber product on water binding
529    properties. Food Hydrocoll. 41, 281–289. doi:10.1016/j.foodhyd.2014.04.020

530 Zheng, C., Sun, D.-W., Zheng, L., 2006. Recent developments and applications of image features for food quality evaluation and inspection – a
531    review. Trends Food Sci. Technol. 17, 642–655. doi:10.1016/j.tifs.2006.06.005

532 Zorrilla, S.E., Singh, R.P., 2003. Heat transfer in double-sided cooking of meat patties considering two-dimensional geometry and radial
533    shrinkage. J. Food Eng. 57, 57–65. doi:10.1016/S0260-8774(02)00273-X

534